

## Modelling laser ultrasound waveforms: The effect of varying pulse duration and material properties

Srinath Rajagopal and Ben T. Cox

Citation: [The Journal of the Acoustical Society of America](#) **149**, 2040 (2021); doi: 10.1121/10.0003558

View online: <https://doi.org/10.1121/10.0003558>

View Table of Contents: <https://asa.scitation.org/toc/jas/149/3>

Published by the [Acoustical Society of America](#)

---

### ARTICLES YOU MAY BE INTERESTED IN

[Modelling and measurement of laser-generated focused ultrasound: Can interventional transducers achieve therapeutic effects?](#)

The Journal of the Acoustical Society of America **149**, 2732 (2021); <https://doi.org/10.1121/10.0004302>

[Acoustics modelling of open-cell foam materials from microstructure and constitutive properties](#)

The Journal of the Acoustical Society of America **149**, 2016 (2021); <https://doi.org/10.1121/10.0003824>

[Laser-induced synthetic aperture ultrasound imaging](#)

Journal of Applied Physics **128**, 163105 (2020); <https://doi.org/10.1063/5.0023412>

[Allan Pierce and adiabatic normal modes](#)

The Journal of the Acoustical Society of America **149**, R5 (2021); <https://doi.org/10.1121/10.0003595>

[Active acoustic cloaking and illusions of sound-hard bodies using the boundary element method](#)

The Journal of the Acoustical Society of America **149**, 1803 (2021); <https://doi.org/10.1121/10.0003556>

[A Fourier transform formulation for radiation from an un baffled cylinder](#)

The Journal of the Acoustical Society of America **148**, 2311 (2020); <https://doi.org/10.1121/10.0002258>

---



**Advance your science and career  
as a member of the**

**ACOUSTICAL SOCIETY OF AMERICA**

LEARN MORE



## Modelling laser ultrasound waveforms: The effect of varying pulse duration and material properties

Srinath Rajagopal<sup>1,a)</sup> and Ben T. Cox<sup>2,b)</sup>

<sup>1</sup>*Ultrasound and Underwater Acoustics, National Physical Laboratory, Hampton Road, Teddington, TW11 0LW, United Kingdom*

<sup>2</sup>*Department of Medical Physics and Biomedical Engineering, University College London, Malet Place Engineering Building, Gower Street, London, WC1E 6BT, United Kingdom*

### ABSTRACT:

Optical generation of ultrasound using nanosecond duration laser pulses has generated great interest both in industrial and biomedical applications. The availability of portable laser devices using semiconductor technology and optical fibres, as well as numerous source material types based on nanocomposites, has proliferated the applications of laser ultrasound. The nanocomposites can be deposited on the tip of optical fibres as well as planar hard and soft backing materials using various fabrication techniques, making devices suitable for a variety of applications. The ability to choose the acoustic material properties and the laser pulse duration gives considerable control over the ultrasound output. Here, an analytical time-domain solution is derived for the acoustic pressure waveform generated by a planar optical ultrasound source consisting of an optically absorbing layer on a backing. It is shown that by varying the optical attenuation coefficient, the thickness of the absorbing layer, the acoustic properties of the materials, and the laser pulse duration, a wide variety of pulse shapes and trains can be generated. It is shown that a source with a reflecting backing can generate pulses with higher amplitude than a source with an acoustically-matched backing in the same circumstances when stress-confinement has not been satisfied.

© 2021 Author(s). All article content, except where otherwise noted, is licensed under a Creative Commons Attribution (CC BY) license (<http://creativecommons.org/licenses/by/4.0/>). <https://doi.org/10.1121/10.0003558>

(Received 3 October 2020; revised 21 January 2021; accepted 29 January 2021; published online 25 March 2021)

[Editor: Martin D. Verweij]

Pages: 2040–2054

### I. INTRODUCTION

Laser pulses have been used to generate broadband ultrasonic pulses since soon after the first Q-switched laser was developed.<sup>1</sup> This *photoacoustic effect* is now widely exploited, in particular for industrial testing and inspection,<sup>2,3</sup> in picosecond ultrasonics,<sup>4</sup> and for biomedical imaging.<sup>5</sup> More recently, ultrasound generated from optically absorbing polymer nanocomposites has gained attention<sup>6,7</sup> for applications including all-optical ultrasound imaging,<sup>8,9</sup> ablative therapy,<sup>10</sup> array transmitters,<sup>11</sup> acoustic kinoforms,<sup>12</sup> and the calibration of medical hydrophones.<sup>13</sup> In particular, carbon-polymer nanocomposites (CPN) have become popular because of the high optical absorption and low quantum yield of carbon nanoparticles, and polydimethylsiloxane (PDMS) has been widely used as a matrix material due to its large thermal expansivity and, therefore, efficient ultrasound generation. Several fabrication techniques have been tested,<sup>14</sup> including electrospinning,<sup>15,16</sup> dip-coating,<sup>17</sup> spin-coating,<sup>16</sup> infiltration,<sup>18</sup> chemical vapor deposition,<sup>19</sup> vacuum filtration,<sup>20</sup> and blade film coating<sup>21</sup> with the aim of producing absorbers that provide pulses that are both very broadband and have large amplitude.

It is the calibration of medical hydrophones that has motivated the current work. In this application, a broadband and planar acoustic source is required with which to test hydrophones using a Primary Standard interferometer at a National Measurement Institute, such as the National Physical Laboratory in the UK. A source comprising a thin optically-absorbing CPN layer deposited on a supporting substrate by blade film coating has been shown to be a promising candidate.<sup>13,21</sup> The aim of this paper is to model the temporal shape of the ultrasound pulse generated by such a source. As the generated wave is required to be planar (at least over a region larger than the sensitive area of the hydrophone being tested), the problem can be modelled as one-dimensional. The acoustic properties of the optically-absorbing layer will typically differ from both the backing substrate and the material (water) into which the ultrasound is transmitted. There will be acoustic reflections at these interfaces, so the layer thickness becomes a length scale in the problem. A second length scale is given by the depth of penetration of the light into the optically-absorbing layer, and a third by the duration of the laser pulse (multiplied by the sound speed). The interaction of these factors will govern the shape of the generated waveform. For instance, it was observed recently that the acoustic pressure amplitude generated by a PDMS CPN source depended significantly on whether it was deposited on an acoustically-reflective backing (glass) or an acoustically-matched (PDMS)

<sup>a)</sup>ORCID: 0000-0001-9627-4353

<sup>b)</sup>Electronic mail: b.cox@ucl.ac.uk; ORCID: 0000-0001-7296-4093.

backing.<sup>22</sup> Interestingly, this implies that the condition of *stress confinement*—isochoric heat deposition—does not hold in this case, and any modelling must take into account the pulse duration and, therefore, how it relates to the other length scales. With the increasing availability of lasers which can offer considerable control over the pulse duration, in particular fibre lasers,<sup>23–25</sup> there is a need for a model that can incorporate these factors explicitly. The effects of varying these factors could then be investigated and current devices analysed (and perhaps novel devices suggested). In this paper, an analytical expression is derived that describes the wide-variety of waveforms that can be generated by a three-layer optical ultrasound source by varying the backing material, pulse duration, layer thickness, and optical penetration depth. The analytical model is compared to a numerical model and is also used to examine how the pulse duration effects the ratio of reflective to matched backing source amplitudes.

## II. ANALYTICAL MODEL

### A. Previous work

When a laser pulse is incident on a CPN absorber, the optical energy absorbed is converted to heat (assuming no radiative decay) and both heat and elastic waves propagate from the heated region. The coupled propagation of heat and elastic waves has received a great deal of attention.<sup>26,27</sup> Fortunately, for our situation, it is possible to make a number of assumptions to simplify the problem. The typical length scales involved here are layers on the order of 10 μm thickness and pulse durations on the order of 1 to hundreds of nanoseconds, and it is therefore not only possible to disregard non-Fourier heat conduction mechanisms<sup>28</sup> but also to neglect heat diffusion, which will occur on a much longer timescale and even then result in low amplitude waves.<sup>29</sup> As the model is one-dimensional, it is also possible to neglect shear waves, so we will treat the materials as fluids. The relevant equation is therefore the photoacoustic wave equation for the acoustic pressure,  $p$ ,

$$\frac{1}{c^2} \frac{\partial^2 p}{\partial t^2} - \frac{\partial^2 p}{\partial x^2} = \frac{\Gamma}{c^2} \frac{\partial \mathcal{H}}{\partial t}, \tag{1}$$

where  $\mathcal{H}(x, t)$  is the absorbed optical power density,  $\Gamma$  is the dimensionless photoacoustic efficiency, and  $c$  is the sound speed. When the photoacoustic source is not moving, as in this case, then the optical power density can be separated as  $\mathcal{H}(x, t) = H(x)f(t)$ , where  $H$  and  $f$  have dimensions of  $\text{J}\cdot\text{m}^{-3}$  and  $\text{s}^{-1}$ , respectively.

The simplest scenario is when there are no acoustic boundaries and the pulse duration is short enough that the heat deposition can be considered to be instantaneous on an acoustic timescale, as the heating function can then be modelled as a delta function in time,  $f(t) = \delta(t)$ . In practice, this is a good assumption when the duration of the laser pulse,  $\tau$ , (taken as indicative of the time to thermalize all the absorbed optical energy as the nonradiative relaxation is

typically fast) is much shorter than the stress relaxation time  $\tau_{ac} = \min(\mu^{-1}, d)/c$ , where  $c$  [ $\text{m}\cdot\text{s}^{-1}$ ] is the sound-speed,  $\mu^{-1}$  [ $\text{m}$ ] is the optical penetration depth, and  $d$  the absorber thickness. (Also, the acoustic pressure amplitude will be maximized under this condition.) In this case, if the absorbing layer extends from  $x = 0$  to  $x = d$ , then the acoustic pressure waveform will be the truncated exponential proportional to  $\exp(-\mu(x - ct))U(x - ct)(1 - U(x - ct - d))$  where  $U$  is the unit step (Heaviside) function. When there is an acoustically reflecting surface at  $x = 0$ , then the concept of an image source can be used to write the waveform as a sum of the above exponential and its reflection about  $x = ct$  weighted by the reflection coefficient,  $R$ .<sup>30</sup> (Reference 31 studies the equivalent spherical case.) When there is also a reflecting surface on the other side of the absorber at  $x = d$  then multiple reflections between the two surfaces must be considered.<sup>32</sup> Finally, when the laser pulse duration is long enough such that stress confinement is not satisfied, it is necessary to convolve these simple waveforms with the laser pulse shape in time to obtain the generated acoustic waveform. The analytical solution for this situation when the pulse is rectangular is derived in the time domain in the following sections.

Some aspects of this problem have been studied in the literature. Reference 32 studied this case for low absorption ( $\mu \ll 1/d$ ) and derived a solution in the frequency domain. Reference 33 found an analytical solution for the case of a Gaussian excitation pulse and an absorbing layer of finite thickness, and considered the relationship between the pulse duration, the layer thickness, and the optical penetration depth, but did not consider the effects of the reflecting boundaries. References 34–36 did consider the acoustic reflections, but only for the case of delta-function excitation. Reference 37 considered the case when the two media surrounding the absorbing layer are the same and derived frequency domain expressions which were numerically Fourier transformed to time series. A frequency-domain, multilayer model that accounts for heat transfer was derived in Ref. 38.

### B. Analytical solution for three-layer model

We consider the case illustrated in Fig. 1, in which a pulse of light travels from the left through transparent medium A into optically-absorbing medium B, where it is absorbed following Beer’s law. The three media have different sound speeds,  $c_A, c_B, c_C$  and characteristic acoustic

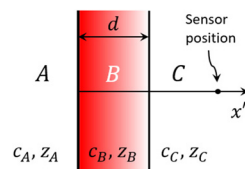


FIG. 1. (Color online) Schematic of the arrangement in which an optical absorber (medium B) of thickness  $d$  with Beer’s law optical absorption is sandwiched between two optically non-absorbing media, A and C. The sound-speeds and acoustic impedances of the three media are,  $c_A, c_B, c_C, z_A, z_B$ , and  $z_C$ .

impedances,  $z_A, z_B, z_C$ . The absorbing medium, B, has thickness  $d$  and optical attenuation coefficient,  $\mu$ . When  $\mu > 1/d$  there will be significant exponential decay of the absorbed energy density across the absorbing region, and for low absorbing B, some of the light will continue on through to the transparent medium C. We aim to model the acoustic pressure reaching a sensor positioned in medium C.

The laser pulse is modelled as a rectangular pulse of duration  $\tau$  and energy per unit area  $E$  irrespective of its duration, so the power per unit area in the pulse is  $E/\tau$ , and its pulse shape,  $f(t)$ , normalized to give an integral of one, is

$$f(t) = \begin{cases} 1/\tau, & -\tau/2 < t < \tau/2, \\ 0, & \text{otherwise.} \end{cases} \quad (2)$$

There are two acoustically-reflecting surfaces—the interfaces between media A and B and between B and C. Since acoustic absorption is not included in this model, the acoustic waves will bounce backward and forward within layer B many times. This can be modelled by using the concept of image sources. For a detector at position  $x > d$ , the absorbed energy density,  $H$ , incorporating the image sources, can be written as

$$H(x) = \begin{cases} 0, & x > d, \\ TH_0 e^{-\mu x}, & 0 < x < d, \\ TH_0 R_A e^{\mu x}, & -d < x < 0, \\ TH_0 R_A R_C e^{-\mu(x+2d)}, & -2d < x < -d, \\ TH_0 R_A^2 R_C e^{\mu(x+2d)}, & -3d < x < -2d, \\ \vdots & \vdots \\ TH_0 (R_A R_C)^{n/2} e^{-\mu(x+nd)}, & -nd < x < -(n-1)d, \quad n = 0, 2, \dots \\ TH_0 R_A^{(n+1)/2} R_C^{(n-1)/2} e^{\mu(x+(n-1)d)}, & -nd < x < -(n-1)d, \quad n = 1, 3, \dots \end{cases} \quad (3)$$

where  $H_0$  is the absorbed energy density at the surface  $x = 0$ ,  $T$  is the acoustic pressure transmission coefficient for a wave travelling from medium B to medium C, and  $R_A$  and  $R_C$  are the acoustic pressure reflection coefficients for waves travelling in medium B and reflected from media A and C, respectively. The even  $n$  terms correspond to the wave that initially sets off in the positive  $x$  direction, and is then multiply-reflected, while the odd  $n$  terms correspond to the wave that sets off in the negative  $x$  direction before being multiply-reflected.

This use of image sources has essentially turned a three-layer problem into a problem of two half-spaces, one with sound speed  $c_B$  containing the photoacoustic source, and the other with sound speed  $c_C$  in which the detector lies. To reduce the problem to one in which there is only a single sound speed, thereby allowing us to use the free-space Green's function to solve it, we let the sound speed everywhere be  $c_B$  and define a virtual detector position  $\hat{x}$  such that  $(\hat{x} - d) = (x - d)(c_B/c_C)$  so that the time of arrival of the

signal is the same as it would have been were the correct sound speeds used.

The solution to Eq. (1) can now be written using the free-space Green's function  $G$  as

$$p(x, t) = \frac{\Gamma}{c_B^2} \int_0^{t^+} \int_{-\infty}^{\infty} G(x, x', t - t') \frac{\partial \mathcal{H}}{\partial t'}(x', t') dx' dt'. \quad (4)$$

Since, from Eq. (2),  $\partial f / \partial t = (\delta(t + \tau/2) - \delta(t - \tau/2)) / \tau$ , Eq. (4) becomes

$$p(x, t) = \frac{\Gamma}{\tau c_B^2} \int_{-\infty}^{\infty} H(x') (G(x, x', t + \tau/2) - G(x, x', t - \tau/2)) dx'. \quad (5)$$

Substituting in the expression for  $H$  from Eq. (3) gives<sup>32</sup>

$$p(x, t) = \frac{\Gamma T H_0}{\tau c_B^2} \left\{ \begin{aligned} & \sum_{n \text{ even}} (R_A R_C)^{n/2} e^{-\mu n d} \int_{-nd}^{-(n-1)d} e^{-\mu x'} (G(x, x', t + \tau/2) - G(x, x', t - \tau/2)) dx' \\ & + \sum_{n \text{ odd}} R_A^{(n+1)/2} R_C^{(n-1)/2} e^{\mu(n-1)d} \int_{-nd}^{-(n-1)d} e^{\mu x'} (G(x, x', t + \tau/2) - G(x, x', t - \tau/2)) dx' \end{aligned} \right\}. \quad (6)$$

The free-space Green's function in one dimension for a virtual detector position  $\hat{x} > x'$  is given by

$$G(x, x', t - t') = \frac{c_B}{2} U\left(t - t' - \frac{(\hat{x} - x')}{c_B}\right) = \frac{c_B}{2} U\left(t - t' - \frac{(d - x')}{c_B} - \frac{(x - d)}{c_C}\right). \quad (7)$$

Therefore, for a detector positioned at  $x > d$ , the acoustic pressure time-series can be written as

$$p(x, t) = \frac{\Gamma TH_0}{2\tau c_B} \left( \sum_{n \text{ even}} (R_A R_C)^{n/2} e^{-\mu n d} I_{n, \text{even}} + \sum_{n \text{ odd}} R_A^{(n+1)/2} R_C^{(n-1)/2} e^{\mu(n-1)d} I_{n, \text{odd}} \right), \quad (8)$$

where

$$I_{n, \text{even}} = \int_{-nd}^{-(n-1)d} e^{-\mu x'} \left( U\left(t + \frac{\tau}{2} - \frac{(d - x')}{c_B} - \frac{(x - d)}{c_C}\right) - U\left(t - \frac{\tau}{2} - \frac{(d - x')}{c_B} - \frac{(x - d)}{c_C}\right) \right) dx', = \int_{-nd}^{-(n-1)d} g_{\text{even}}(x', t) dx', \quad (9)$$

with

$$g_{\text{even}}(x', t) = \begin{cases} e^{-\mu x'}, & -\frac{\tau}{2} + \frac{d - x'}{c_B} + \frac{x - d}{c_C} < t < \frac{\tau}{2} + \frac{d - x'}{c_B} + \frac{x - d}{c_C}, \\ 0, & \text{otherwise,} \end{cases}$$

and

$$I_{n, \text{odd}} = \int_{-nd}^{-(n-1)d} e^{\mu x'} \left( U\left(t + \frac{\tau}{2} - \frac{(d - x')}{c_B} - \frac{(x - d)}{c_C}\right) - U\left(t - \frac{\tau}{2} - \frac{(d - x')}{c_B} - \frac{(x - d)}{c_C}\right) \right) dx', = \int_{-nd}^{-(n-1)d} g_{\text{odd}}(x', t) dx', \quad (10)$$

with

$$g_{\text{odd}}(x', t) = \begin{cases} e^{\mu x'}, & -\frac{\tau}{2} + \frac{d - x'}{c_B} + \frac{x - d}{c_C} < t < \frac{\tau}{2} + \frac{d - x'}{c_B} + \frac{x - d}{c_C}, \\ 0, & \text{otherwise.} \end{cases}$$

These integrals are evaluated in the [Appendix](#) and the resulting expressions are grouped below for when  $\tau < d/c_B$  and  $\tau > d/c_B$ ,

$$I_{n, \text{even}}^{\tau < d/c_B} = \begin{cases} 0, & t < -\frac{\tau}{2} + \frac{nd}{c_B} + \frac{(x - d)}{c_C}, \\ \frac{1}{\mu} \left( e^{-\mu(-c_B\tau/2 + d + (c_B/c_C)(x - d) - c_B t)} - e^{\mu(n-1)d} \right), & -\frac{\tau}{2} + \frac{nd}{c_B} + \frac{(x - d)}{c_C} < t < \frac{\tau}{2} + \frac{nd}{c_B} + \frac{(x - d)}{c_C}, \\ \frac{2}{\mu} e^{-\mu(d + (c_B/c_C)(x - d) - c_B t)} \sinh(\mu c_B \tau / 2), & \frac{\tau}{2} + \frac{nd}{c_B} + \frac{(x - d)}{c_C} < t < -\frac{\tau}{2} + \frac{(n+1)d}{c_B} + \frac{(x - d)}{c_C}, \\ \frac{1}{\mu} \left( e^{\mu n d} - e^{-\mu(c_B\tau/2 + d + (c_B/c_C)(x - d) - c_B t)} \right), & -\frac{\tau}{2} + \frac{(n+1)d}{c_B} + \frac{(x - d)}{c_C} < t < \frac{\tau}{2} + \frac{(n+1)d}{c_B} + \frac{(x - d)}{c_C}, \\ 0, & t > \frac{\tau}{2} + \frac{(n+1)d}{c_B} + \frac{(x - d)}{c_C}. \end{cases} \quad (11)$$

$$I_{n, \text{odd}}^{\tau < d/c_B} = \begin{cases} 0, & t < -\frac{\tau}{2} + \frac{nd}{c_B} + \frac{(x - d)}{c_C}, \\ \frac{1}{\mu} \left( e^{-\mu(n-1)d} - e^{\mu(-c_B\tau/2 + d + (c_B/c_C)(x - d) - c_B t)} \right), & -\frac{\tau}{2} + \frac{nd}{c_B} + \frac{(x - d)}{c_C} < t < \frac{\tau}{2} + \frac{nd}{c_B} + \frac{(x - d)}{c_C}, \\ \frac{2}{\mu} e^{\mu(d + (c_B/c_C)(x - d) - c_B t)} \sinh(\mu c_B \tau / 2), & \frac{\tau}{2} + \frac{nd}{c_B} + \frac{(x - d)}{c_C} < t < -\frac{\tau}{2} + \frac{(n+1)d}{c_B} + \frac{(x - d)}{c_C}, \\ \frac{1}{\mu} \left( e^{\mu(c_B\tau/2 + d + (c_B/c_C)(x - d) - c_B t)} - e^{-\mu n d} \right), & -\frac{\tau}{2} + \frac{(n+1)d}{c_B} + \frac{(x - d)}{c_C} < t < \frac{\tau}{2} + \frac{(n+1)d}{c_B} + \frac{(x - d)}{c_C}, \\ 0, & t > \frac{\tau}{2} + \frac{(n+1)d}{c_B} + \frac{(x - d)}{c_C}. \end{cases} \quad (12)$$

$$I_{n, \text{even}}^{\tau > d/c_B} = \begin{cases} 0, & t < -\frac{\tau}{2} + \frac{nd}{c_B} + \frac{(x-d)}{c_C}, \\ \frac{1}{\mu} (e^{-\mu(-c_B\tau/2+d+(c_B/c_C)(x-d)-c_Bt)} - e^{\mu(n-1)d}), & -\frac{\tau}{2} + \frac{nd}{c_B} + \frac{(x-d)}{c_C} < t < -\frac{\tau}{2} + \frac{(n+1)d}{c_B} + \frac{(x-d)}{c_C}, \\ \frac{1}{\mu} (e^{\mu nd} - e^{\mu(n-1)d}), & -\frac{\tau}{2} + \frac{(n+1)d}{c_B} + \frac{(x-d)}{c_C} < t < \frac{\tau}{2} + \frac{nd}{c_B} + \frac{(x-d)}{c_C}, \\ \frac{1}{\mu} (e^{\mu nd} - e^{-\mu(c_B\tau/2+d+(c_B/c_C)(x-d)-c_Bt)}), & \frac{\tau}{2} + \frac{nd}{c_B} + \frac{(x-d)}{c_C} < t < \frac{\tau}{2} + \frac{(n+1)d}{c_B} + \frac{(x-d)}{c_C}, \\ 0, & t > \frac{\tau}{2} + \frac{(n+1)d}{c_B} + \frac{(x-d)}{c_C}. \end{cases} \quad (13)$$

$$I_{n, \text{odd}}^{\tau > d/c_B} = \begin{cases} 0, & t < -\frac{\tau}{2} + \frac{nd}{c_B} + \frac{(x-d)}{c_C}, \\ \frac{1}{\mu} (e^{-\mu(n-1)d} - e^{\mu(-c_B\tau/2+d+(c_B/c_C)(x-d)-c_Bt)}), & -\frac{\tau}{2} + \frac{nd}{c_B} + \frac{(x-d)}{c_C} < t < -\frac{\tau}{2} + \frac{(n+1)d}{c_B} + \frac{(x-d)}{c_C}, \\ \frac{1}{\mu} (e^{-\mu(n-1)d} - e^{-\mu nd}), & -\frac{\tau}{2} + \frac{(n+1)d}{c_B} + \frac{(x-d)}{c_C} < t < \frac{\tau}{2} + \frac{nd}{c_B} + \frac{(x-d)}{c_C}, \\ \frac{1}{\mu} (e^{\mu(c_B\tau/2+d+(c_B/c_C)(x-d)-c_Bt)} - e^{-\mu nd}), & \frac{\tau}{2} + \frac{nd}{c_B} + \frac{(x-d)}{c_C} < t < \frac{\tau}{2} + \frac{(n+1)d}{c_B} + \frac{(x-d)}{c_C}, \\ 0, & t > \frac{\tau}{2} + \frac{(n+1)d}{c_B} + \frac{(x-d)}{c_C}. \end{cases} \quad (14)$$

Equations (8) and (11)–(14) give the solution to Eq. (1) for the set-up shown in Fig. 1.

### C. Simplified models

#### 1. Weakly absorbing, multi-layer

In the weakly absorbing limit, when  $\mu \ll 1/d$  and the absorbed energy density  $H_0 e^{-\mu x} \approx E/d$  in Eq. (3), the solution takes the simpler form,

$$p(x, t) = \frac{\Gamma TE}{2d\tau c_B} \left( \sum_{n \text{ even}} (R_A R_C)^{n/2} I_n + \sum_{n \text{ odd}} R_A^{(n+1)/2} R_C^{(n-1)/2} I_n \right), \quad (15)$$

$$I_n^{\tau < d/c_B} = \begin{cases} 0, & t < -\frac{\tau}{2} + \frac{nd}{c_B} + \frac{(x-d)}{c_C}, \\ c_B \left( t + \frac{\tau}{2} \right) - nd - \frac{c_B}{c_C} (x-d), & -\frac{\tau}{2} + \frac{nd}{c_B} + \frac{(x-d)}{c_C} < t < \frac{\tau}{2} + \frac{nd}{c_B} + \frac{(x-d)}{c_C}, \\ c_B \tau, & \frac{\tau}{2} + \frac{nd}{c_B} + \frac{(x-d)}{c_C} < t < -\frac{\tau}{2} + \frac{(n+1)d}{c_B} + \frac{(x-d)}{c_C}, \\ -c_B \left( t - \frac{\tau}{2} \right) + (n+1)d + \frac{c_B}{c_C} (x-d), & -\frac{\tau}{2} + \frac{(n+1)d}{c_B} + \frac{(x-d)}{c_C} < t < \frac{\tau}{2} + \frac{(n+1)d}{c_B} + \frac{(x-d)}{c_C}, \\ 0, & t > \frac{\tau}{2} + \frac{(n+1)d}{c_B} + \frac{(x-d)}{c_C}, \end{cases} \quad (16)$$

$$I_n^{\tau > d/c_B} = \begin{cases} 0, & t < -\frac{\tau}{2} + \frac{nd}{c_B} + \frac{(x-d)}{c_C}, \\ c_B \left( t + \frac{\tau}{2} \right) - nd - \frac{c_B}{c_C} (x-d), & -\frac{\tau}{2} + \frac{nd}{c_B} + \frac{(x-d)}{c_C} < t < -\frac{\tau}{2} + \frac{(n+1)d}{c_B} + \frac{(x-d)}{c_C}, \\ d, & -\frac{\tau}{2} + \frac{(n+1)d}{c_B} + \frac{(x-d)}{c_C} < t < \frac{\tau}{2} + \frac{nd}{c_B} + \frac{(x-d)}{c_C}, \\ -c_B \left( t - \frac{\tau}{2} \right) + (n+1)d + \frac{c_B}{c_C} (x-d), & \frac{\tau}{2} + \frac{nd}{c_B} + \frac{(x-d)}{c_C} < t < \frac{\tau}{2} + \frac{(n+1)d}{c_B} + \frac{(x-d)}{c_C}, \\ 0, & t > \frac{\tau}{2} + \frac{(n+1)d}{c_B} + \frac{(x-d)}{c_C}. \end{cases} \quad (17)$$

2. Weakly absorbing, two-layer

When, in addition, the absorber and the medium into which it is transmitting are acoustically the same,  $z_B = z_C$ ,  $c_B = c_C = c$ , there is no reverberation, and the solution simplifies further to

$$p(x, t) = \frac{\Gamma E}{2d\tau c} (I_0 + R_A I_1), \tag{18}$$

$$I_0^{\tau < d/c} = \begin{cases} 0, & t < \frac{x-d}{c} - \frac{\tau}{2}, \\ d-x+c(t+\tau/2), & \frac{x-d}{c} - \frac{\tau}{2} < t < \frac{x-d}{c} + \frac{\tau}{2}, \\ c\tau, & \frac{x-d}{c} + \frac{\tau}{2} < t < \frac{x}{c} - \frac{\tau}{2}, \\ x-c(t-\tau/2), & \frac{x}{c} - \frac{\tau}{2} < t < \frac{x}{c} + \frac{\tau}{2}, \\ 0, & t > \frac{x}{c} + \frac{\tau}{2}, \end{cases} \tag{19}$$

$$I_0^{\tau > d/c} = \begin{cases} 0, & t < \frac{x-d}{c} - \frac{\tau}{2}, \\ d-x+c(t+\tau/2), & \frac{x-d}{c} - \frac{\tau}{2} < t < \frac{x}{c} - \frac{\tau}{2}, \\ d, & \frac{x}{c} - \frac{\tau}{2} < t < \frac{x-d}{c} + \frac{\tau}{2}, \\ x-c(t-\tau/2), & \frac{x-d}{c} + \frac{\tau}{2} < t < \frac{x}{c} + \frac{\tau}{2}, \\ 0, & t > \frac{x}{c} + \frac{\tau}{2}, \end{cases} \tag{20}$$

$$I_1^{\tau < d/c} = \begin{cases} 0, & t < \frac{x}{c} - \frac{\tau}{2}, \\ c(t+\tau/2) - x, & \frac{x}{c} - \frac{\tau}{2} < t < \frac{x}{c} + \frac{\tau}{2}, \\ c\tau, & \frac{x}{c} + \frac{\tau}{2} < t < \frac{x+d}{c} - \frac{\tau}{2}, \\ d+x-c(t-\tau/2), & \frac{x+d}{c} - \frac{\tau}{2} < t < \frac{x+d}{c} + \frac{\tau}{2}, \\ 0, & t > \frac{x+d}{c} + \frac{\tau}{2}, \end{cases} \tag{21}$$

$$I_1^{\tau > d/c} = \begin{cases} 0, & t < \frac{x}{c} - \frac{\tau}{2}, \\ c(t+\tau/2) - x, & \frac{x}{c} - \frac{\tau}{2} < t < \frac{x+d}{c} - \frac{\tau}{2}, \\ d, & \frac{x+d}{c} - \frac{\tau}{2} < t < \frac{x}{c} + \frac{\tau}{2}, \\ d+x-c(t-\tau/2), & \frac{x}{c} + \frac{\tau}{2} < t < \frac{x+d}{c} + \frac{\tau}{2}, \\ 0, & t > \frac{x+d}{c} + \frac{\tau}{2}. \end{cases} \tag{22}$$

D. Effect of backing on maximum amplitude

In laser-generated ultrasound, the localized increase in pressure following the light absorption will, over time, propagate away as an acoustic wave. A short laser pulse leads to efficient laser generation of ultrasound when the localized pressure increase does not have time to completely leave the region into which the energy is being deposited while it is being deposited—hence the term stress confinement—and so the acoustic pressure builds up. When the stress confinement condition is not met, the acoustic pressure due to the early-arriving part of the optical pulse will have left the absorbing region before the latter parts are thermalized; the acoustic pressure spreads out, rather than builds up, and therefore the maximum amplitude decreases as the laser pulse duration increases.

Consider the case of two acoustically-identical half-spaces, left and right, the right-hand one of which is optically absorbing. When a plane wave pulse of light, short enough for stress confinement to be satisfied, is incident normally through the non-absorbing medium onto the absorbing medium as in Fig. 1, it generates a pressure profile that resembles the profile of the absorbed optical energy.<sup>39</sup> In this case, this initial acoustic pressure distribution will divide into two equal parts, one propagating to the left the other to the right. Now, if the half-space on the left were replaced by a material with a different acoustic impedance, glass say, then a proportion of the left-going wave will be reflected back and immediately follow the right-going wave. Therefore, the pressure-pulse generated from a CPN source backed by an acoustic reflector will be twice as long as that of a source with a backing acoustically matched to the CPN source. Note, though, that the maximum amplitude will remain unchanged.<sup>39</sup> When the optical pulse is longer than the stress confinement requirement, however, the left-going wave will be reflected by the glass back to the right during the continued optical deposition of heat and there will be a consequent build-up of pressure in the absorbing region. If the reflection is positive, the total acoustic pressure reached will be higher than it would be in the absence of the reflection.

We can be more specific. For the low absorption, two-layer case, the ratio of the amplitude with reflective or matched backings can be found straightforwardly from Eqs. (18)–(22). In the stress confined condition,  $\tau < d/c$ , the maximum amplitudes are the same, so the ratio is 1. For pulse durations  $d/c < \tau < 2d/c$ , the ratio increases linearly with  $\tau$  from 1 to  $(1 + R_A)$ . When  $\tau > 2d/c$ , there is at least one instance at which the amplitude of both  $I_0$  and  $I_1$  are going to be maximum, and thus the ratio equals  $(1 + R_A)$ .

These results can be generalised to the three-layered case and hold for both low and high absorption. There are three cases:

- When the backing is negatively reflecting,  $z_A < z_B$ , e.g., in the case of an air-backed source, then the maximum amplitude that can be obtained is the same as for the matched backing case ( $z_A = z_B$ ). This holds both when  $z_B > z_C$  and  $z_B < z_C$ .

- When  $z_A > z_B > z_C$ , as in the case of a glass-backed epoxy-based source transmitting into water, then the amplitude reaches  $(1 + R_A)$  times the amplitude in the matched-backing case (as for the two-layer case above).
- In the case of a low-impedance absorber,  $z_A > z_B < z_C$ , as in the case of a glass-backed PDMS-based source transmitting into water, then the amplitude ratio continues to grow with the pulse duration  $\tau$  such that

$$\lim_{\tau \rightarrow \infty} \left( \frac{\max(p_{\text{reflecting}})}{\max(p_{\text{matched}})} \right) \rightarrow \frac{1 + R_A}{1 - R_A R_C}, \quad (23)$$

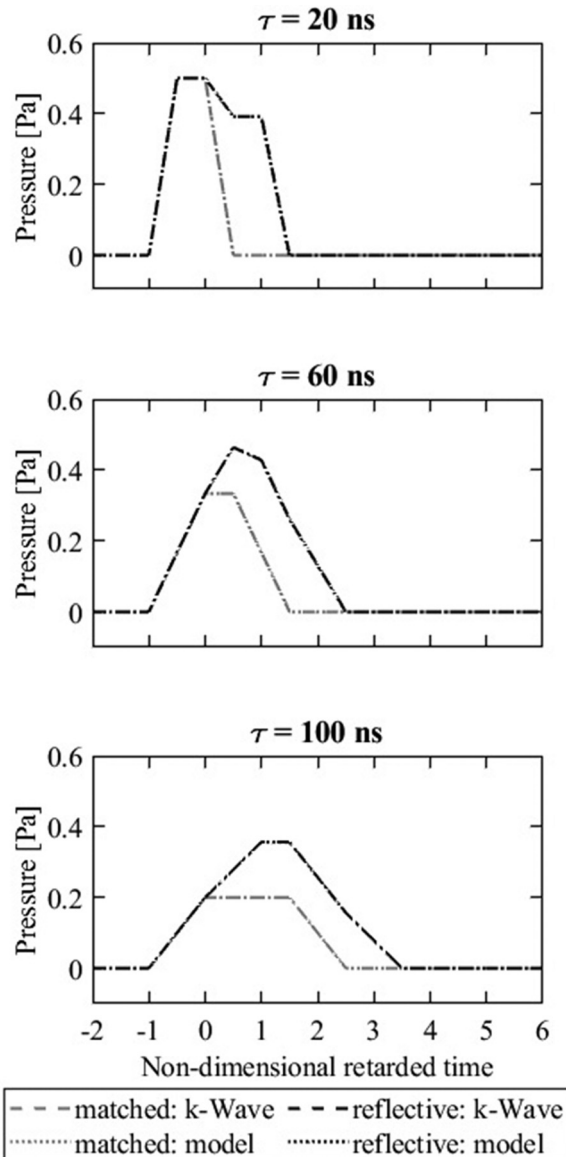


FIG. 2. Weakly absorbing, two-layer model. Analytical solutions, Eqs. (18)–(22), and k-Wave simulations showing acoustic pressure waveforms for sources with reflective and matched backings, for laser pulse durations ranging from stress-confined ( $\tau < d/c$ ) to unconfined ( $\tau > d/c$ ). The thickness of the optical absorber was  $60 \mu\text{m}$ , the sound-speed in medium B was  $c = 1500 \text{ m}\cdot\text{s}^{-1}$  and the acoustic relaxation time,  $\tau_{\text{ac}} = d/c$ , was  $40 \text{ ns}$ . The waveforms are plotted against non-dimensional retarded time,  $\{t - (\text{position}_{\text{sensor}} - d)/c - (d/c) + \tau/2\}/(d/c)$ .

as can be seen by summing the geometric series in Eq. (15). In many practical cases, the convergence is quite fast, and values close to this limit are reached for  $\tau \approx 10 d/c_B$ .

### III. EXAMPLES

In this section, the analytical solution derived above is plotted for various cases and compared to numerical simulations using k-Wave, a third-party open-source wave solver for MATLAB (MathWorks, Inc., Natick, MA), which is designed for modelling the propagation of broadband acoustic waves in the time-domain.<sup>40</sup> The comparison shows that the time series from the analytical formulae agree with a conventional numerical wave-solver, and indeed could be used as a test-case for this and other numerical wave-solvers.

#### A. Weakly absorbing, two-layer model

The analytical solution, Eqs. (18)–(22), was compared against numerical simulations using k-Wave. Medium A was set to have the acoustic properties of glass and medium B (and therefore C) was water. The thickness of the optical absorbing region B was  $60 \mu\text{m}$ . The absorbed optical energy density was assumed uniform across the absorbing region. The laser pulse duration  $\tau$ , spanned 20–100 ns. For each pulse duration, two solutions were computed to test the effect of the backing, i.e., in the first simulation, all media were water (matched case) and in the second simulation medium A was glass, and media B and C were water. The nominal sound-speeds and densities of glass and water were  $5500 \text{ m}\cdot\text{s}^{-1}$ ,  $1500 \text{ m}\cdot\text{s}^{-1}$ ,  $2250 \text{ kg}\cdot\text{m}^{-3}$ , and  $1000 \text{ kg}\cdot\text{m}^{-3}$ , respectively. A convergence test was run to ensure that the spatial grid point spacing ( $125 \text{ nm}$ ) and time step ( $8.33 \text{ ps}$ ) were small enough such that numerical artifacts were negligible. The waveforms were recorded at  $512 \mu\text{m}$  from the

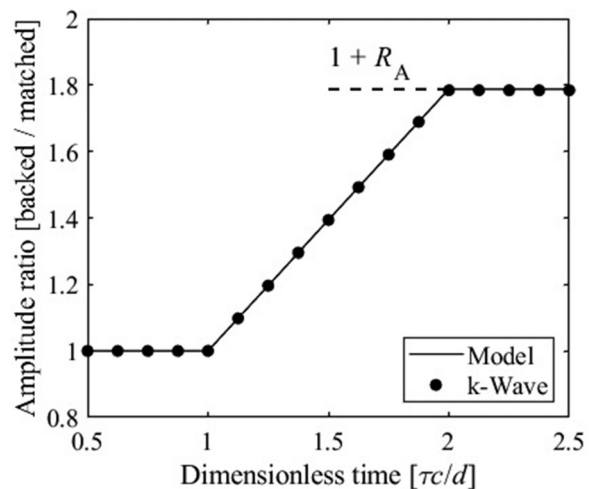


FIG. 3. Weakly-absorbing, two-layer model. Ratio of the maximum amplitude in the reflecting and matched-backing cases for laser pulse durations from 20 to 100 ns, which is plotted against the non-dimensionalised time  $\tau c/d$ .  $R_A$  is the pressure reflection coefficient for a wave travelling in the absorber and reflected from the backing,  $d = 60 \mu\text{m}$  is the absorber thickness, and  $c = 1500 \text{ m}\cdot\text{s}^{-1}$  is the sound-speed in the optical absorber. k-Wave simulations were performed in steps of 5 ns pulse duration.



interface between media B and C (the edge of the absorbing region). Figure 2 shows example waveforms, and the ratios of the maximum amplitudes are shown in Fig. 3. In these simulations, as in those below, k-Wave's output agrees very closely with the analytical solution. (In fact, the level of agreement is limited only by memory and time available to run the k-Wave simulations.)

**B. Three-layer model**

In this section, the analytical solution, Eqs. (8) and (11)–(14), was compared against numerical k-Wave simulations for several different scenarios.

First, the analytical solutions for the air-backed  $z_A < z_B$  case were computed with  $z_B < z_C$  and  $z_B > z_C$ . The nominal sound-speeds of air (medium A), optical absorber (medium B), and water (medium C) were  $343 \text{ m} \cdot \text{s}^{-1}$ ,  $1000 \text{ m} \cdot \text{s}^{-1}$  (PDMS) or  $2500 \text{ m} \cdot \text{s}^{-1}$  (epoxy), and  $1500 \text{ m} \cdot \text{s}^{-1}$ , respectively, and their densities were  $1.2 \text{ kg} \cdot \text{m}^{-3}$ ,  $1000 \text{ kg} \cdot \text{m}^{-3}$  (PDMS) or  $1250 \text{ kg} \cdot \text{m}^{-3}$  (epoxy), and  $1000 \text{ kg} \cdot \text{m}^{-3}$ , respectively. The thickness,  $d$  of the optical absorber, medium B, was  $50 \mu\text{m}$ . Two values of the optical attenuation coefficient  $\mu$  were compared: in the first case it was  $10^5 \text{ m}^{-1}$  ( $1/\mu < d$ ) and in the second case, it was  $10^4 \text{ m}^{-1}$  ( $1/\mu > d$ ). The laser pulse duration,  $\tau$ , spanned 1–1000 ns, and its amplitude,  $1/\tau$ . The maximum value of the number of reflections was chosen to

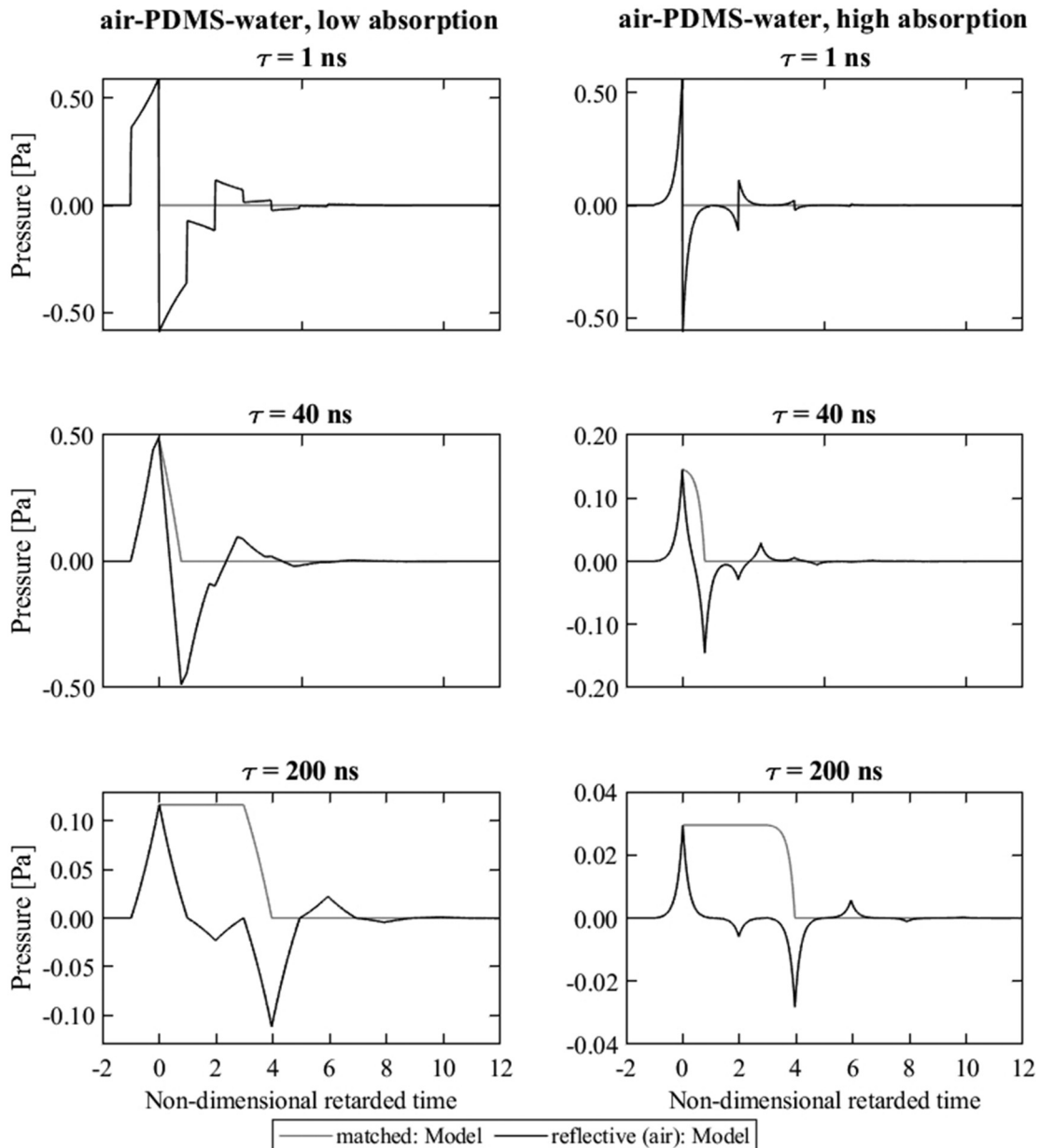


FIG. 4. Analytical solutions for the three-layer model, Eqs. (8) and (11)–(14), for sources with matched and air backings for laser pulse durations ranging from stress-confined ( $\tau < d/c_B$ ) to unconfined ( $\tau > d/c_B$ ). The thickness of the optical absorber,  $d$  was  $50 \mu\text{m}$  and the two optical penetration depths ( $1/\mu$ ) were  $100 \mu\text{m}$  (left panel) and  $10 \mu\text{m}$  (right panel). The corresponding acoustic relaxation time,  $\tau_{ac} = d/c_B$  was  $50 \text{ ns}$  (left panel) and  $\tau_{ac} = \mu^{-1}/c_B$  was  $10 \text{ ns}$  (right panel). The acoustic impedance of the optical absorber,  $z_B$  was less than the acoustic impedance of water,  $z_C$ . In the negatively reflecting case  $z_A < z_B$ , the impedance of the air backing, and in the matched case  $z_A = z_B$ .

be the lowest value for which an increase would make no visible change in the output time series. k-Wave simulations were not performed for this case as the presence of the air-absorber interface leads to slow convergence with grid step size. The resulting waveforms are shown in Figs. 4 and 5. The waveforms are plotted against non-dimensional retarded time,  $\{t - (position_{sensor} - d)/c_C - (d/c_B) + \tau/2\}/(d/c_B)$ .

Second, the analytical solutions and k-Wave simulations for the hard-reflective backing,  $z_A > z_B$ , were computed. The medium A was set to have the acoustic properties of glass with sound-speed and density of  $5500 \text{ m} \cdot \text{s}^{-1}$  and  $2250 \text{ kg} \cdot \text{m}^{-3}$ , respectively. The other parameters of the

medium B and medium C were the same as the air-backed case. The resulting waveforms are shown in Figs. 6 and 7. The waveforms are plotted against non-dimensional retarded time,  $\{t - (position_{sensor} - d)/c_C - (d/c_B) + \tau/2\}/(d/c_B)$ .

It is interesting to see that many different pulse shapes can be generated by varying the acoustic impedance,  $z$ , thickness of the optical absorber,  $d$ , optical penetration depth,  $1/\mu$ , and duration of the laser pulse,  $\tau$ . In the case of matched backing,  $z_A = z_B$ , the wave transmitted in medium C is always a singular positive pulse. However, in the case of  $z_A < z_B$  (air-backed) and  $z_A > z_B$  (hard-reflective backing), the polarity of the interfacial reflections will affect the

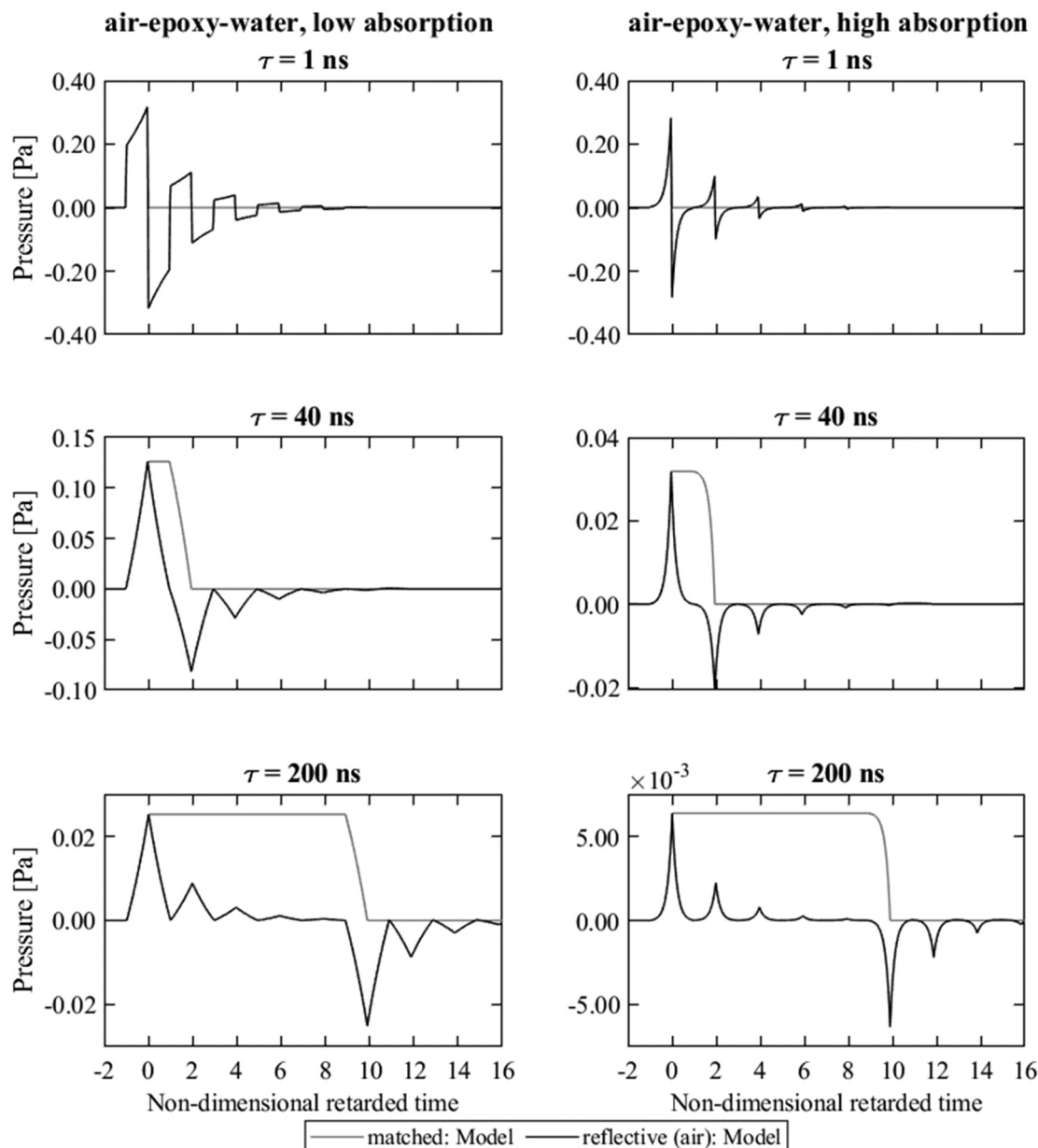


FIG. 5. Analytical solutions for the three-layer model, Eqs. (8) and (11)–(14), for sources with matched and air backings for laser pulse durations ranging from stress-confined ( $\tau < d/c_B$ ) to unconfined ( $\tau > d/c_B$ ). The thickness of the optical absorber,  $d$  was  $50 \mu\text{m}$  and the two optical penetration depths ( $1/\mu$ ) were  $100 \mu\text{m}$  (left panel) and  $10 \mu\text{m}$  (right panel). The corresponding acoustic relaxation time,  $\tau_{ac} = d/c_B$  was  $20 \text{ ns}$  (left panel) and  $\tau_{ac} = \mu^{-1}/c_B$  was  $4 \text{ ns}$  (right panel). The acoustic impedance of the optical absorber,  $z_B$  was greater than the acoustic impedance of water,  $z_C$ . In the negatively reflecting case  $z_A < z_B$ , the impedance of the air backing, and in the matched case  $z_A = z_B$ .

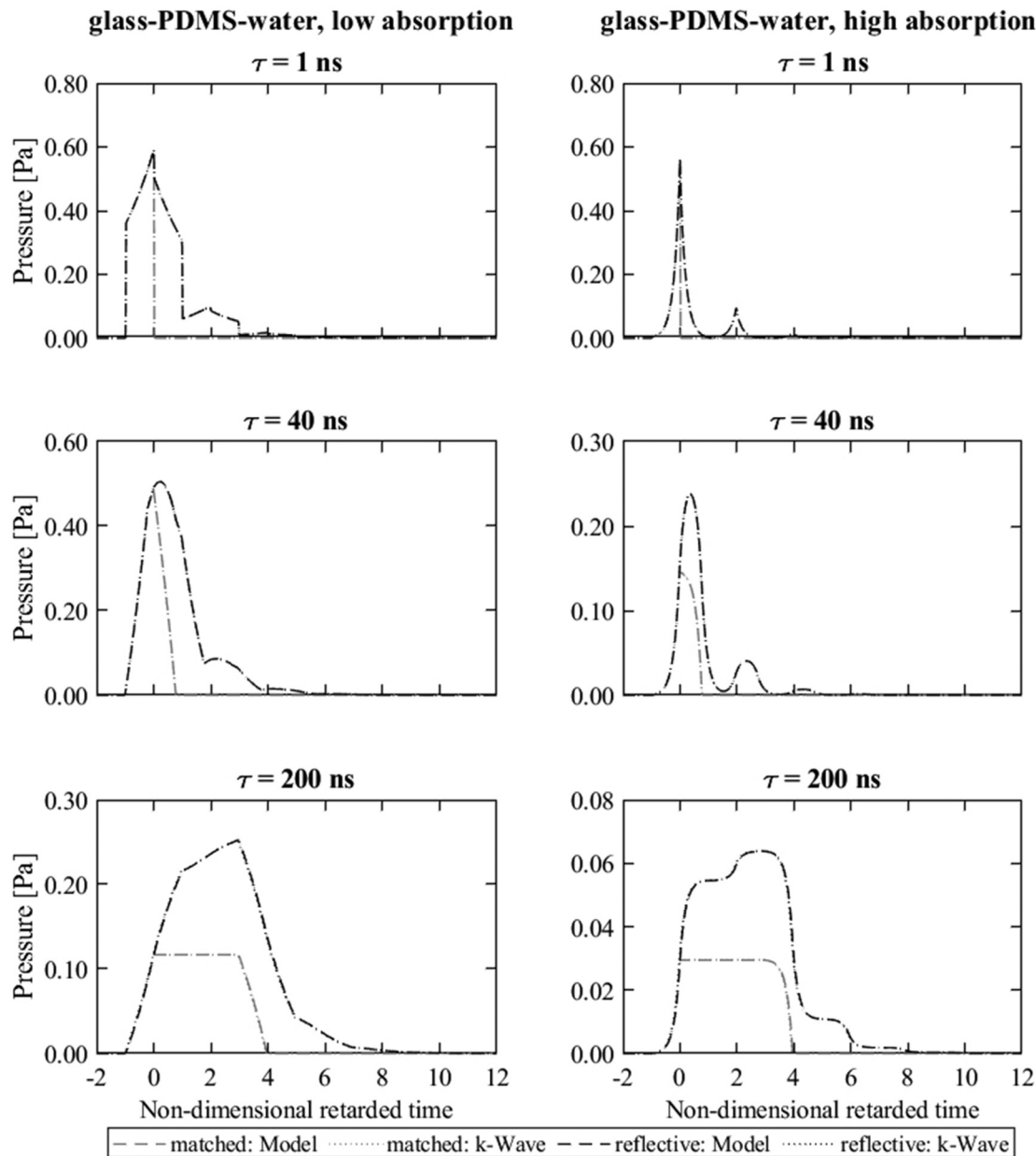


FIG. 6. Analytical solutions for the three-layer model, Eqs. (8) and (11)–(14), and k-Wave simulations showing acoustic pressure waveforms for sources with hard-reflective and matched backings, for laser pulse durations ranging from stress-confined ( $\tau < d/c_B$ ) to unconfined ( $\tau > d/c_B$ ). The thickness of the optical absorber,  $d$  was  $50 \mu\text{m}$  and the two optical penetration depths ( $1/\mu$ ) were  $100 \mu\text{m}$  (left panel) and  $10 \mu\text{m}$  (right panel). The corresponding acoustic relaxation time,  $\tau_{ac} = d/c_B$  was  $50 \text{ ns}$  (left panel) and  $\tau_{ac} = \mu^{-1}/c_B$  was  $10 \text{ ns}$  (right panel). The acoustic impedance of the optical absorber,  $z_B$  was less than the acoustic impedance of water,  $z_C$ . In the reflecting case  $z_B < z_A$ , the impedance of the glass backing, and in the matched case  $z_A = z_B$ .

shape of the wave transmitted into medium C. The shape of the main pulse is also influenced by  $\tau$  when  $\tau > d/c_B$ , since the reflections either add constructively ( $z_B < z_C$ ) or destructively ( $z_B > z_C$ ) with the main pulse giving rise to a multitude of shapes in comparison to the matched backing case as seen in Figs. 4 and 7. Also, the pulse amplitudes are higher for the weakly-absorbing case  $1/\mu > d$  (Figs. 4 and 7; left-panel) compared to the more absorbing case  $1/\mu < d$  (Figs. 4 and 7; right-panel) when  $\tau > d/c_B$ . This is because in the weakly-absorbing case, the reflections interact more frequently with the non-reflected pulse during continued optical deposition of the heat, leading to greater build-up of pressure.

Finally, the effect on the wave amplitude of having a reflective backing, as opposed to a matched backing, was studied and compared to the results from Sec. II D. For laser pulse durations from 1 to 1000 ns, waveforms for the matched backing,  $z_A = z_B$ , and hard-reflective backing,  $z_A > z_B$ , were evaluated. A convergence test was run to ensure that the spatial grid point spacing and time step, at 50 nm and 2 ps, were small enough. For the analytical solution, ten image sources were included in the computations ( $n = 10$ ). The waveforms were recorded at 1.1663 mm from the edge of the optical absorber in water (although the model is one-dimensional, linear, and non-absorbing so would give the same result at any position in medium C).

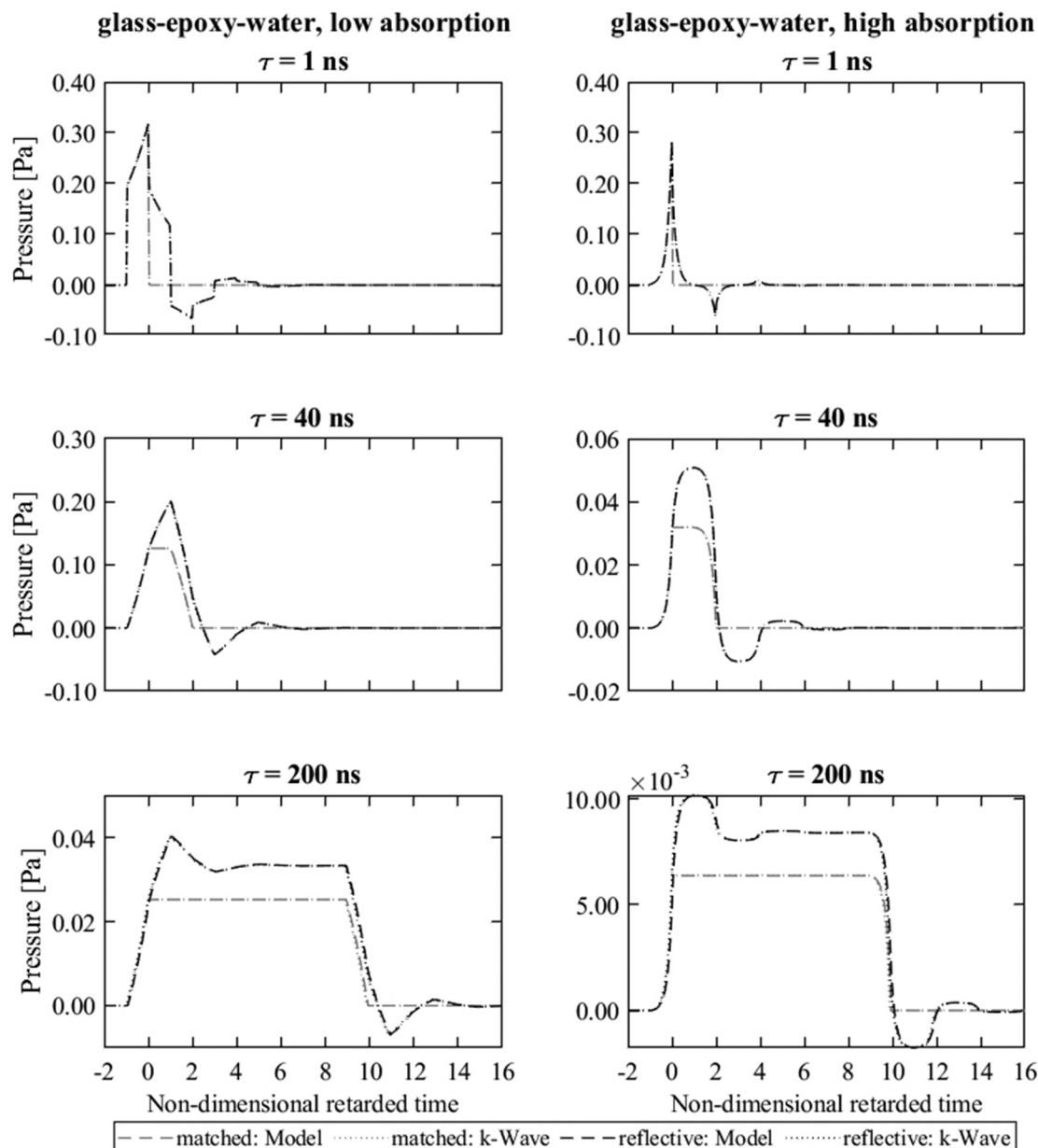


FIG. 7. Analytical solutions for the three-layer model, Eqs. (8) and (11)–(14), and k-Wave simulations showing acoustic pressure waveforms for sources with hard-reflective and matched backings for laser pulse durations ranging from stress-confined ( $\tau < d/c_B$ ) to unconfined ( $\tau > d/c_B$ ). The thickness of the optical absorber,  $d$  was  $50 \mu\text{m}$  and the two optical penetration depths ( $1/\mu$ ) were  $100 \mu\text{m}$  (left panel) and  $10 \mu\text{m}$  (right panel). The corresponding acoustic relaxation time,  $\tau_{ac} = d/c_B$  was  $20 \text{ ns}$  (left panel) and  $\tau_{ac} = \mu^{-1}/c_B$  was  $4 \text{ ns}$  (right panel). The acoustic impedance of the optical absorber,  $z_B$  was greater than the acoustic impedance of water,  $z_C$ . In the reflecting case,  $z_B < z_A$ , the impedance of the glass backing, and in the matched case,  $z_A = z_B$ .

The ratios of the maximum amplitudes are shown in Fig. 8, showing how the ratios approach the long-pulse-duration limits derived in Sec. II D. The “kinks” in the ratio curve in Fig. 8(B), in the case of the PDMS absorber (lower impedance than the water), occur when the duration of the source heating is long enough that the first part of the pulse has propagated through the PDMS, reflected from the PDMS/water interface, propagated back through the PDMS, reflected from the PDMS/glass interface, and is added to by the ongoing heating pulse. When the heating is restricted to the surface of the absorber (very high absorption) these kinks occur at times corresponding to multiples of two round trips through the PDMS layer. When the absorption

depth is greater, as here, the kinks will occur at slightly later times.

A MATLAB® script of the analytical solutions Eqs. (8) and (11)–(14), which can be used to reproduce waveforms in Figs. 4–7 is provided as supplementary material.<sup>42</sup> The supplied example script also produces amplitude spectra of the waveforms in Figs. 4–7.

#### IV. SUMMARY

A time-domain solution was derived in one dimension for the acoustic pressure waveform generated by an optical ultrasound source consisting of an optically absorbing layer

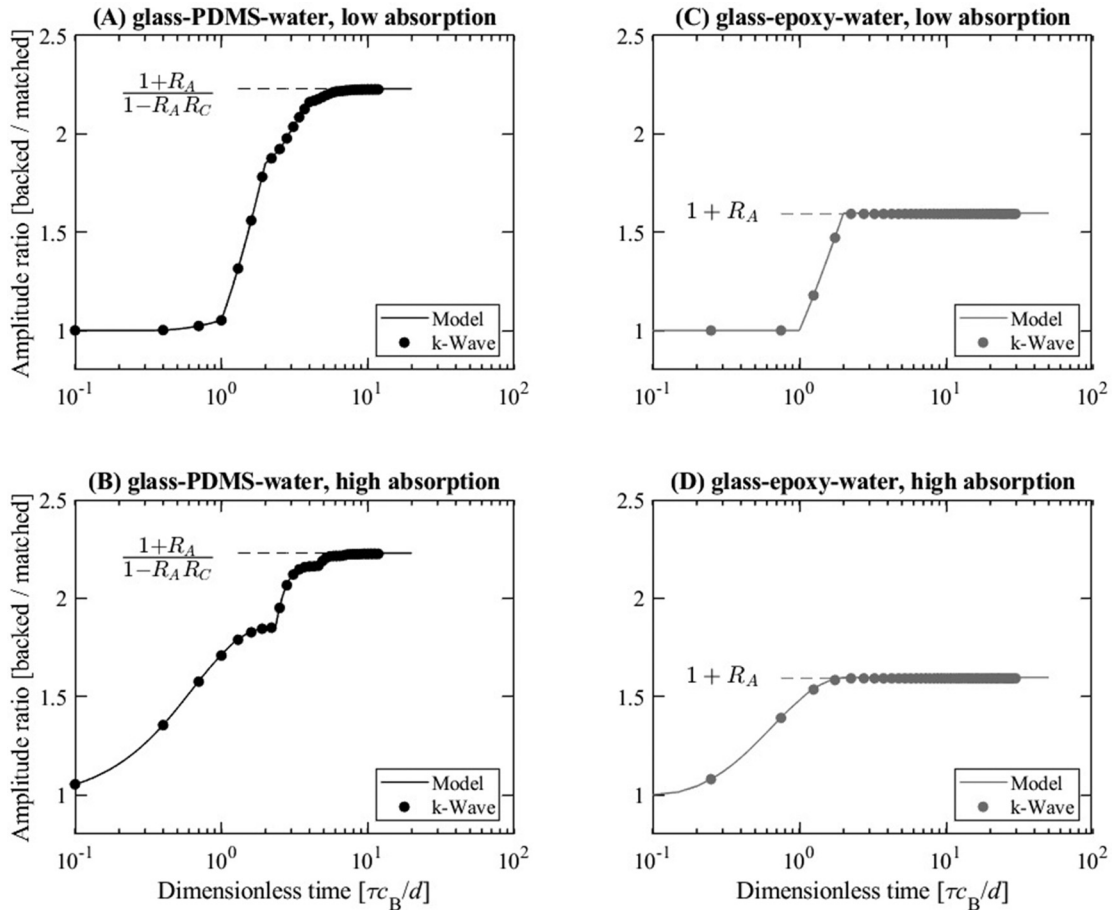


FIG. 8. Three layer model. Ratio of the maximum amplitudes in the hard-reflecting and matched-backing cases against dimensionless time ( $\tau c_B/d$ ) for the four cases: (A)  $z_B < z_C$ ,  $\mu < 1/d$ , (B)  $z_B < z_C$ ,  $\mu > 1/d$ , (C)  $z_B > z_C$ ,  $\mu < 1/d$ , (D)  $z_B > z_C$ ,  $\mu > 1/d$ . k-Wave results are plotted every 15 ns up to 600 ns. The limiting values, which are related purely to the reflection coefficients, are also indicated.

on a backing. It was shown that by varying the optical attenuation coefficient, the thickness of the absorbing layer, the acoustic properties of the materials, and the laser pulse duration, a wide variety of pulse shapes can be generated. It was shown that a source with a reflecting backing can generate pulses with higher amplitude than a similar source with an acoustically-matched backing when stress-confinement has not been satisfied. Analytical expressions for the difference in the amplitudes were found. The analytical model was shown to agree with a widely-used numerical model, k-Wave. While such a numerical model can be used to study much more general cases, an analytical model has no issues with numerical convergence, is faster to compute, requires much less memory, is less prone to user error, and, being in analytical form, can provide greater insight into what is going on—as seen with the expressions for the amplitude ratio derived in Sec. II D. This latter point can be very helpful if the model is to be used as a design tool. A limitation of this work is the neglect of acoustic attenuation. This can be high in CPNs, leading in some cases to the use of very thin optically absorbing layers for which stress confinement does not hold. When this is the case, the effect of the pulse duration on the signal—an effect captured by this model—will become more significant. There has been great interest in

multi-layered optical ultrasound sources for both industrial and biomedical applications, and it is hoped that this work will assist in understanding the characteristics of those sources and in the design of novel optical ultrasound sources.

**ACKNOWLEDGMENTS**

S.R. thanks the UK Department for Business, Energy & Industrial Strategy’s funding of the National Measurement System. B.T.C. acknowledges the European Union’s Horizon 2020 research and innovation program H2020 ICT 2016–2017 under Grant Agreement No. 732411, which is an initiative of the Photonics Public Private Partnership.

**APPENDIX**

This appendix gives details about the solution of the integrals in Eqs. (9) and (10).<sup>41</sup> The regions of integration are shown in Figs. 9 and 10 for the cases when  $\tau < d/c_B$  and  $\tau > d/c_B$ , respectively. The integrand shown (in red) has an exponential decay in the  $x'$  direction, which corresponds to the even  $n$  case. For the case of odd  $n$ , the exponential will decay in the opposite direction. The expressions for the five regions of integration when  $\tau < d/c_B$  and  $\tau > d/c_B$  are derived. First, with the even  $n$  case for  $\tau < d/c_B$ ,

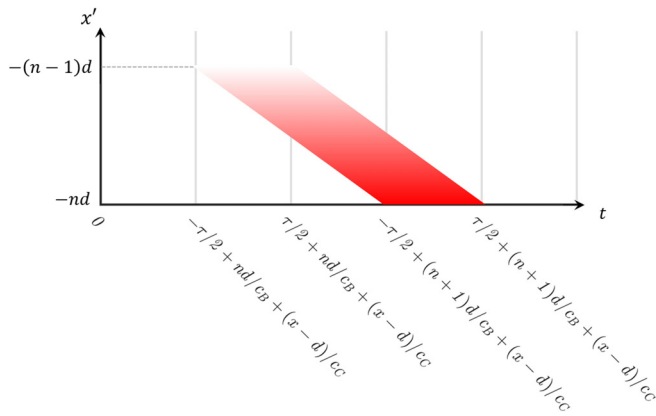


FIG. 9. (Color online) Integrand and region of integration for  $I_{n, \text{even}}$  when  $\tau < d/c_B$  (stress-confined).

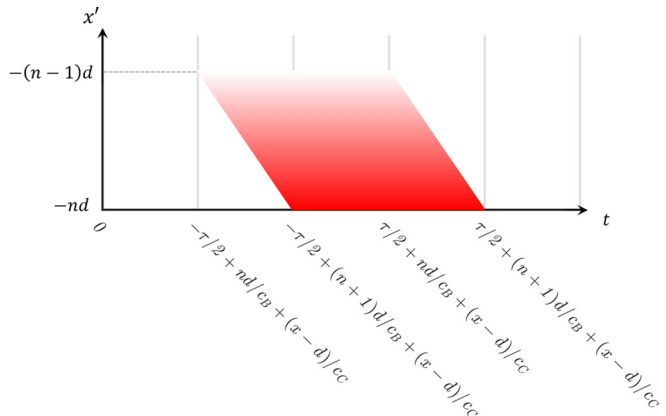


FIG. 10. (Color online) Integrand and region of integration for  $I_{n, \text{even}}$  when  $\tau > d/c_B$  (not stress-confined).

$$I_{n, \text{even}}^{\tau < d/c} = \begin{cases} 0, & t < -\frac{\tau}{2} + \frac{nd}{c_B} + \frac{(x-d)}{c_C}, \\ f_{\text{even},1}, & -\frac{\tau}{2} + \frac{nd}{c_B} + \frac{(x-d)}{c_C} < t < \frac{\tau}{2} + \frac{nd}{c_B} + \frac{(x-d)}{c_C}, \\ f_{\text{even},2}, & \frac{\tau}{2} + \frac{nd}{c_B} + \frac{(x-d)}{c_C} < t < -\frac{\tau}{2} + \frac{(n+1)d}{c_B} + \frac{(x-d)}{c_C}, \\ f_{\text{even},3}, & -\frac{\tau}{2} + \frac{(n+1)d}{c_B} + \frac{(x-d)}{c_C} < t < \frac{\tau}{2} + \frac{(n+1)d}{c_B} + \frac{(x-d)}{c_C}, \\ 0, & t > \frac{\tau}{2} + \frac{(n+1)d}{c_B} + \frac{(x-d)}{c_C}, \end{cases} \quad (\text{A1})$$

$$f_{\text{even},1} = \int_{-nd - c_B \tau/2 + (n+1)d + (c_B/c_C)(x-d) - c_B t}^{-(n-1)d} e^{-\mu x'} dx', \\ = \frac{1}{\mu} \left( -e^{-\mu(n-1)d} + e^{-\mu(-nd - c_B \tau/2 + (n+1)d + (c_B/c_C)(x-d) - c_B t)} \right), \quad (\text{A2})$$

$$f_{\text{even},2} = \int_{-nd - c_B \tau/2 + (n+1)d + (c_B/c_C)(x-d) - c_B t}^{-nd + c_B \tau/2 + (n+1)d + (c_B/c_C)(x-d) - c_B t} e^{-\mu x'} dx', \\ = \frac{2}{\mu} e^{-\mu(d + (c_B/c_C)(x-d) - c_B t)} \sinh(\mu c_B \tau/2), \quad (\text{A3})$$

$$f_{\text{even},3} = \int_{-nd}^{-nd + c_B \tau/2 + (n+1)d + (c_B/c_C)(x-d) - c_B t} e^{-\mu x'} dx', \\ = \frac{1}{\mu} \left( -e^{-\mu(c_B \tau/2 + d + (c_B/c_C)(x-d) - c_B t)} + e^{\mu nd} \right). \quad (\text{A4})$$

For the even  $n$  case for  $\tau > d/c_B$ ,

$$I_{n, \text{even}}^{\tau > d/c} = \begin{cases} 0, & t < -\frac{\tau}{2} + \frac{nd}{c_B} + \frac{(x-d)}{c_C}, \\ f_{\text{even},1}, & -\frac{\tau}{2} + \frac{nd}{c_B} + \frac{(x-d)}{c_C} < t < -\frac{\tau}{2} + \frac{(n+1)d}{c_B} + \frac{(x-d)}{c_C}, \\ f_{\text{even},2}, & -\frac{\tau}{2} + \frac{(n+1)d}{c_B} + \frac{(x-d)}{c_C} < t < \frac{\tau}{2} + \frac{nd}{c_B} + \frac{(x-d)}{c_C}, \\ f_{\text{even},3}, & \frac{\tau}{2} + \frac{nd}{c_B} + \frac{(x-d)}{c_C} < t < \frac{\tau}{2} + \frac{(n+1)d}{c_B} + \frac{(x-d)}{c_C}, \\ 0, & t > \frac{\tau}{2} + \frac{(n+1)d}{c_B} + \frac{(x-d)}{c_C}. \end{cases} \quad (\text{A5})$$

$f_{\text{even},1}$  and  $f_{\text{even},3}$  are unchanged from the  $\tau < d/c_B$  case, but  $f_{\text{even},2}$  needs evaluating,

$$\begin{aligned}
 f_{\text{even},2} &= \int_{-nd}^{-(n-1)d} e^{-\mu x'} dx', \\
 &= \frac{1}{\mu} (e^{\mu nd} - e^{\mu(n-1)d}).
 \end{aligned}
 \tag{A6}$$

Repeating the above calculations for the odd  $n$  case, remembering the exponential in the integrand decays in the opposite direction, gives

$$I_{n,\text{odd}}^{\tau < d/c} = \begin{cases} 0, & t < -\frac{\tau}{2} + \frac{nd}{c_B} + \frac{(x-d)}{c_C}, \\ f_{\text{odd},1}, & -\frac{\tau}{2} + \frac{nd}{c_B} + \frac{(x-d)}{c_C} < t < \frac{\tau}{2} + \frac{nd}{c_B} + \frac{(x-d)}{c_C}, \\ f_{\text{odd},2}, & \frac{\tau}{2} + \frac{nd}{c_B} + \frac{(x-d)}{c_C} < t < -\frac{\tau}{2} + \frac{(n+1)d}{c_B} + \frac{(x-d)}{c_C}, \\ f_{\text{odd},3}, & -\frac{\tau}{2} + \frac{(n+1)d}{c_B} + \frac{(x-d)}{c_C} < t < \frac{\tau}{2} + \frac{(n+1)d}{c_B} + \frac{(x-d)}{c_C}, \\ 0, & t > \frac{\tau}{2} + \frac{(n+1)d}{c_B} + \frac{(x-d)}{c_C}, \end{cases}
 \tag{A7}$$

$$\begin{aligned}
 f_{\text{odd},1} &= \int_{-nd - c_B\tau/2 + (n+1)d + (c_B/c_C)(x-d) - c_Bt}^{-(n-1)d} e^{\mu x'} dx', \\
 &= \frac{1}{\mu} (e^{-\mu(n-1)d} - e^{\mu(-nd - c_B\tau/2 + (n+1)d + (c_B/c_C)(x-d) - c_Bt)}),
 \end{aligned}
 \tag{A8}$$

$$\begin{aligned}
 f_{\text{odd},2} &= \int_{-nd - c_B\tau/2 + (n+1)d + (c_B/c_C)(x-d) - c_Bt}^{-nd + c_B\tau/2 + (n+1)d + (c_B/c_C)(x-d) - c_Bt} e^{\mu x'} dx', \\
 &= \frac{2}{\mu} e^{\mu(d + (c_B/c_C)(x-d) - c_Bt)} \sinh(\mu c_B\tau/2),
 \end{aligned}
 \tag{A9}$$

$$\begin{aligned}
 f_{\text{odd},3} &= \int_{-nd}^{-nd + c_B\tau/2 + (n+1)d + (c_B/c_C)(x-d) - c_Bt} e^{\mu x'} dx', \\
 &= \frac{1}{\mu_a} (e^{\mu(-nd + c_B\tau/2 + (n+1)d + (c_B/c_C)(x-d) - c_Bt)} - e^{-\mu nd}).
 \end{aligned}
 \tag{A10}$$

And finally,

$$I_{n,\text{odd}}^{\tau > d/c} = \begin{cases} 0, & t < -\frac{\tau}{2} + \frac{nd}{c_B} + \frac{(x-d)}{c_C}, \\ f_{\text{odd},1}, & -\frac{\tau}{2} + \frac{nd}{c_B} + \frac{(x-d)}{c_C} < t < -\frac{\tau}{2} + \frac{(n+1)d}{c_B} + \frac{(x-d)}{c_C}, \\ f_{\text{odd},2}, & -\frac{\tau}{2} + \frac{(n+1)d}{c_B} + \frac{(x-d)}{c_C} < t < \frac{\tau}{2} + \frac{nd}{c_B} + \frac{(x-d)}{c_C}, \\ f_{\text{odd},3}, & \frac{\tau}{2} + \frac{nd}{c_B} + \frac{(x-d)}{c_C} < t < \frac{\tau}{2} + \frac{(n+1)d}{c_B} + \frac{(x-d)}{c_C}, \\ 0, & t > \frac{\tau}{2} + \frac{(n+1)d}{c_B} + \frac{(x-d)}{c_C}. \end{cases}
 \tag{A11}$$

$f_{\text{odd},1}$  and  $f_{\text{odd},3}$  are unchanged from the  $\tau < d/c_B$  case, but  $f_{\text{odd},2}$  needs to be evaluated

$$\begin{aligned}
 f_{\text{odd},2} &= \int_{-nd}^{-(n-1)d} e^{\mu x'} dx', \\
 &= \frac{1}{\mu_a} (e^{-\mu(n-1)d} - e^{\mu nd}).
 \end{aligned}
 \tag{A12}$$

These results are grouped together in Eqs. (11)–(14).

- <sup>1</sup>E. F. Carome, N. A. Clark, and C. E. Moeller, "Generation of acoustic signals in liquids by ruby laser-induced thermal stress transients," *Appl. Phys. Lett.* **4**, 95–97 (1964).
- <sup>2</sup>L. E. Scruby and C. B. Drain, *Laser Ultrasonics Techniques and Applications* (Adam Hilger, Bristol, UK, 1990).
- <sup>3</sup>V. E. Gusev, Z. Shen, and T. W. Murray, "Special issue on laser ultrasonics," *Appl. Sci.* **9**, 5561 (2019).
- <sup>4</sup>O. Matsuda, M. C. Larciprete, R. L. Voti, and O. B. Wright, "Fundamentals of picosecond laser ultrasonics," *Ultrasonics* **56**, 3–20 (2015).
- <sup>5</sup>S. Manohar and D. Razansky, "Photoacoustics: A historical review," *Adv. Opt. Photon.* **8**, 586–617 (2016).
- <sup>6</sup>S.-L. Chen, "Review of laser-generated ultrasound transmitters and their applications to all-optical ultrasound transducers and imaging," *Appl. Sci.* **7**, 25 (2016).
- <sup>7</sup>T. Lee, H. W. Baac, Q. Li, and L. J. Guo, "Efficient Photoacoustic Conversion in Optical Nanomaterials and Composites," *Adv. Opt. Mater.* **6**, 1800491 (2018).
- <sup>8</sup>E. J. Alles, S. Noimark, E. Maneas, E. Z. Zhang, I. P. Parkin, P. C. Beard, and A. E. Desjardins, "Video-rate all-optical ultrasound imaging," *Biomed. Opt. Exp.* **9**, 3481–3494 (2018).
- <sup>9</sup>E. Vannacci, S. Granchi, L. Belsito, A. Roncaglia, and E. Biagi, "Wide bandwidth fiber-optic ultrasound probe in MOMS technology: Preliminary signal processing results," *Ultrasonics* **75**, 164–173 (2017).
- <sup>10</sup>H. W. Baac, J. Frampton, J. G. Ok, S. Takayama, and L. J. Guo, "Localized micro-scale disruption of cells using laser-generated focused ultrasound," *J. Biophoton.* **6**, 905–910 (2013).
- <sup>11</sup>T. Buma, M. Spisar, and M. O'Donnell, "A high-frequency, 2-D array element using thermoelastic expansion in PDMS," *IEEE Trans. Ultrason. Ferroelectr. Freq. Control* **50**, 1161–1176 (2003).
- <sup>12</sup>M. D. Brown, D. I. Nikitichev, B. E. Treeby, and B. T. Cox, "Generating arbitrary ultrasound fields with tailored optoacoustic surface profiles," *Appl. Phys. Lett.* **110**, 094102–094105 (2017).
- <sup>13</sup>S. Rajagopal and B. T. Cox, "100 MHz bandwidth planar laser-generated ultrasound source for hydrophone calibration," *Ultrasonics* **108**, 106218 (2020).
- <sup>14</sup>S. Noimark, R. J. Colchester, R. K. Poduval, E. Maneas, E. J. Alles, T. Zhao, E. Z. Zhang, M. Ashworth, E. Tsolaki, A. H. Chester, N. Latif, S. Bertazzo, A. L. David, S. Ourselin, P. C. Beard, I. P. Parkin, I. Papakonstantinou, and A. E. Desjardins, "Polydimethylsiloxane composites for optical ultrasound generation and multimodality imaging," *Adv. Funct. Mater.* **28**, 1704919 (2018).
- <sup>15</sup>R. K. Poduval, S. Noimark, R. J. Colchester, T. J. Macdonald, I. P. Parkin, A. E. Desjardins, and I. Papakonstantinou, "Optical fiber ultrasound transmitter with electrospun carbon nanotube-polymer composite," *Appl. Phys. Lett.* **110**, 223701 (2017).
- <sup>16</sup>B. Y. Hsieh, J. Kim, J. Zhu, S. Li, X. Zhang, and X. Jiang, "A laser ultrasound transducer using carbon nanofibers-polydimethylsiloxane composite thin film," *Appl. Phys. Lett.* **106**, 021902 (2015).
- <sup>17</sup>S. Noimark, R. J. Colchester, B. J. Blackburn, E. Z. Zhang, E. J. Alles, S. Ourselin, P. C. Beard, I. Papakonstantinou, I. P. Parkin, and A. E. Desjardins, "Carbon-nanotube-PDMS composite coatings on optical fibers for all-optical ultrasound imaging," *Adv. Funct. Mater.* **26**, 8390–8396 (2016).
- <sup>18</sup>W. Y. Chang, W. Huang, J. Kim, S. Li, and X. Jiang, "Candle soot nanoparticles-polydimethylsiloxane composites for laser ultrasound transducers," *Appl. Phys. Lett.* **107**, 161903 (2015).
- <sup>19</sup>Z. Chen, Y. Wu, Y. Yang, J. Li, B. Xie, X. Li, S. Lei, J. Ou-Yang, X. Yang, Q. Zhou, and B. Zhu, "Multilayered carbon nanotube yarn based optoacoustic transducer with high energy conversion efficiency for ultrasound application," *Nano Energy* **46**, 314–321 (2018).
- <sup>20</sup>C. Moon, X. Fan, K. Ha, and D. Kim, "Generation of planar blast waves using carbon nanotubes-poly-dimethylsiloxane optoacoustic transducer," *AIP Adv.* **7**, 015107 (2017).
- <sup>21</sup>S. Rajagopal, T. Sainsbury, B. E. Treeby, and B. T. Cox, "Laser generated ultrasound sources using carbon-polymer nanocomposites for high frequency metrology," *J. Acoust. Soc. Am.* **144**, 584–597 (2018).
- <sup>22</sup>S. Rajagopal, B. E. Treeby, and B. T. Cox, "Effect of backing on carbon-polymer nanocomposite sources for laser generation of broadband ultrasound pulses," in *Proceedings of the 2018 IEEE International Ultrasonics Symposium*, Kobe, Japan (October 22–25, 2018), pp. 1–4.
- <sup>23</sup>T. J. Allen and P. C. Beard, "Pulsed near-infrared laser diode excitation system for biomedical photoacoustic imaging," *Opt. Lett.* **31**, 3462–3464 (2006).
- <sup>24</sup>D. J. Richardson, J. Nilsson, and W. A. Clarkson, "High power fiber lasers: Current status and future perspectives [Invited]," *J. Opt. Soc. Am. B* **27**, B63–B92 (2010).
- <sup>25</sup>A. Malinowski, P. Gorman, C. A. Codemard, F. Ghiringhelli, A. J. Boyland, A. Marshall, M. N. Zervas, and M. K. Durkin, "High-peak-power, high-energy, high-average-power pulsed fiber laser system with versatile pulse duration and shape," *Opt. Lett.* **38**, 4686–4689 (2013).
- <sup>26</sup>J. Ignaczak and M. Ostoja-Starzewski, *Thermoelasticity with Finite Wave Speeds* (Oxford University Press, Oxford, UK, 2009).
- <sup>27</sup>B. Straughan, *Heat Waves* (Springer, New York, 2011).
- <sup>28</sup>A. A. Minakov and C. Schick, "Nanoscale heat conduction in CNT-POLYMER nanocomposites at fast thermal perturbations," *Molecules* **24**, 2794 (2019).
- <sup>29</sup>E. Gutiérrez-Reyes, C. García-Segundo, A. García-Valenzuela, R. Ortega, C. Buj, and F. Filbir, "Heat transport considerations in the mathematical analysis of the photoacoustic and photothermal effects," *J. Phys. Commun.* **3**, 085007 (2019).
- <sup>30</sup>S. M. Park, M. I. Khan, H. Z. Cheng, and G. J. Diebold, "Photoacoustic effect in strongly absorbing fluids," *Ultrasonics* **29**, 63–67 (1991).
- <sup>31</sup>G. J. Diebold, "Photoacoustic waves at reflecting interfaces," *Rev. Sci. Instrum.* **74**, 801–804 (2003).
- <sup>32</sup>M. I. Khan, T. Sun, and G. J. Diebold, "Photoacoustic waves generated by absorption of laser radiation in optically thin layers," *J. Acoust. Soc. Am.* **93**, 1417–1425 (1993).
- <sup>33</sup>D. Cywiak, M. D. Barreiro-Argüelles, M. Cywiak, A. Landa-Curiel, C. Garcia-Segundo, and G. Gutierrez-Juárez, "A one-dimensional solution of the photoacoustic wave equation and its relationship with optical absorption," *Int. J. Thermophys.* **34**, 1473–1480 (2013).
- <sup>34</sup>F. Herrerías-Azcué, A. González-Vega, J. Torres-Arenas, and G. Gutiérrez-Juárez, "Solution for the photoacoustic wave equation with a single spatial degree of freedom, Beer's law absorption of radiation and mechanical barriers," *Mod. Phys. Lett. B* **27**, 1350135 (2013).
- <sup>35</sup>Q. Shan, A. Kuhn, P. A. Payne, and R. J. Dewhurst, "Characterisation of laser-ultrasound signals from an optical absorption layer within a transparent fluid," *Ultrasonics* **34**, 629–639 (1996).
- <sup>36</sup>E. Svanström, T. Linder, and T. Löfqvist, "Analytical one-dimensional model for laser-induced ultrasound in planar optically absorbing layer," *Ultrasonics* **54**, 888–893 (2014).
- <sup>37</sup>N. Baddour and A. Mandelis, "The effect of acoustic impedance on sub-surface absorber geometry reconstruction using 1D frequency-domain photoacoustics," *Photoacoustics* **3**, 132–142 (2015).
- <sup>38</sup>H. Hu, W. Zhang, J. Xu, and Y. Dong, "General analytical solution for photoacoustic effect with multilayers," *Appl. Phys. Lett.* **92**, 014103 (2008).
- <sup>39</sup>G. J. Diebold, "Chapter 1 photoacoustic monopole radiation: Waves from objects with symmetry in one, two, and three dimensions," in *Photoacoustic Imaging and Spectroscopy*, 1st. ed., edited by L. V. Wang (CRC Press, Boca Raton, FL, 2009), p. 536.
- <sup>40</sup>B. E. Treeby and B. T. Cox, "k-Wave: MATLAB toolbox for the simulation and reconstruction of photoacoustic wave fields," *J. Biomed. Opt.* **15**, 021314 (2010).
- <sup>41</sup>S. Rajagopal, *Laser-Generated, Plane-Wave, Broadband Ultrasound Sources for Metrology* (University College London, London, 2020).
- <sup>42</sup>See supplementary material at <https://www.scitation.org/doi/suppl/10.1121/10.0003558> for a matlab® function script, which implements analytical solutions Eqs. (11)–(14) and the accompanying matlab® example script that reproduces analytical waveforms in Figs. 4–7.